Applied Catalysis B: Environmental 170-171 (2015) 301–311

Contents lists available at ScienceDirect

Applied Catalysis B: Environmental

journal homepage: www.elsevier.com/locate/apcatb

# β-SiC alveolar foams as a structured photocatalytic support for the gas phase photocatalytic degradation of methylethylketone

Romain Masson, Valérie Keller, Nicolas Keller*

*Institut de Chimie et Procédés pour l'Energie, l'Environnement et la Santé (ICPEES), CNRS UMR 7515, Université de Strasbourg, 25 rue Becquerel, 67087 Strasbourg, France*

ARTICLE INFO

*Article history:*
Received 22 October 2014
Received in revised form 21 January 2015
Accepted 23 January 2015
Available online 7 February 2015

*Keywords:*
Photocatalysis
β-SiC alveolar foam
Support
$TiO_2$
Methylethylketone

ABSTRACT

Alveolar open-cell self-bonded β-SiC foams with medium specific surface area and large mean cell size were used as high open porosity structured support for $TiO_2$ in the gas phase photocatalytic degradation of methylethylketone. The influence of parameters such as the $TiO_2$ weight content and the foam mean cell size, as well as both methylethylketone concentration and air flow rate was investigated. The structured $TiO_2$/β-SiC foam photocatalytic material takes advantage of the static mixer role played by the β-SiC foam support and of its ability to increase the amount of $TiO_2$ per unit reactor volume. The value of using $TiO_2$/β-SiC foams for structuring flow-through reactors was highlighted in comparison to the commercial Quartzel photocatalytic felt standard and thin film coated wall reactor, the gain in performances being all the more pronounced that the pollutant concentration and the air flow rate were low.



## 1. Introduction

In parallel to the search for high efficiency photocatalysts, the future of gas-phase photocatalysis as air remediation treatment requires that the photocatalysts are able to operate according to criteria meeting the constraints of industrial implementation [1]. One strategy deals with the replacement of powdery photocatalysts by photocatalytic media, through the immobilization of the photocatalyst on a macroscopic support material in the reactor for using more efficiently the reactor volume and increasing the surface-to-reactor volume ratio in comparison to reactors operating in a thin film coated-wall mode [2–4]. In addition, the replacement of a powdery photocatalyst by an easy-to-handle photocatalytic media provides also a secure environment for both photocatalyst handling and recycling.

The design of a photocatalytic media is driven by the need to overcome – or at least minimize – intrinsic drawbacks directly issued from the immobilization of the photocatalyst on a macroscopic body within the photoreactor: namely, (i) low exposed surface area-to-volume ratios, (ii) possible mass transfer limitations, (iii) increase in pressure drops within the catalytic reactor, (iv) complexity in providing the light to the photocatalyst and to the core of the reactor especially, and (v) possible catalyst washout or fouling related to the photocatalyst/support adherence.

Within the search for new photocatalytic media, porous or multichannel support materials such as honeycomb-shaped or square channel monoliths, have gained interest for combining the need for a good contact between the photocatalyst and the air, to the necessity to process high flow rates at a low pressure drop [5,6]. However, they suffer from poor irradiation distribution with a limited penetration depth within the monolith [7].

In thermal catalysis, solid alveolar foams have been shown to benefit from their high porosity (0.60–0.95) for reducing the pressure drop along the catalyst bed as well as from suitable mass transfer properties for overcoming some of the drawbacks of conventional packed bed reactors [8,9]. Recently, in the wake of the interest they received as support in thermal catalysis, three-dimensionally ordered porous solid alveolar foams attracted growing attention in photocatalysis and were reported to be a very interesting structural support for use as photocatalytic filters [3] for their capacity to increase the light penetration within the monolithic reactors and their ability to process high flow rates with very low pressure drops. They consist of cellular monoliths characterized by the geometric structure of the cells (*i.e.*, shape and size) and the way they are distributed, their most characteristic parameters being the cell size, the strut or bridge diameter and the window size or pore diameter [10,11]. A recent model developed for β-SiC foams by Edouard based on the packing of regular pentagonal dodecahedron (Fig. 1A), revealed to be quite close to the real structure of a unit cell of solid foam [12].

The use of β-SiC alveolar foams as structured photocatalyst support remains scarce in comparison to that of metallic and ceramic

* Corresponding author. Tel.: +33 368852811.
*E-mail address:* nkeller@unistra.fr (N. Keller).

http://dx.doi.org/10.1016/j.apcatb.2015.01.030
0926-3373/

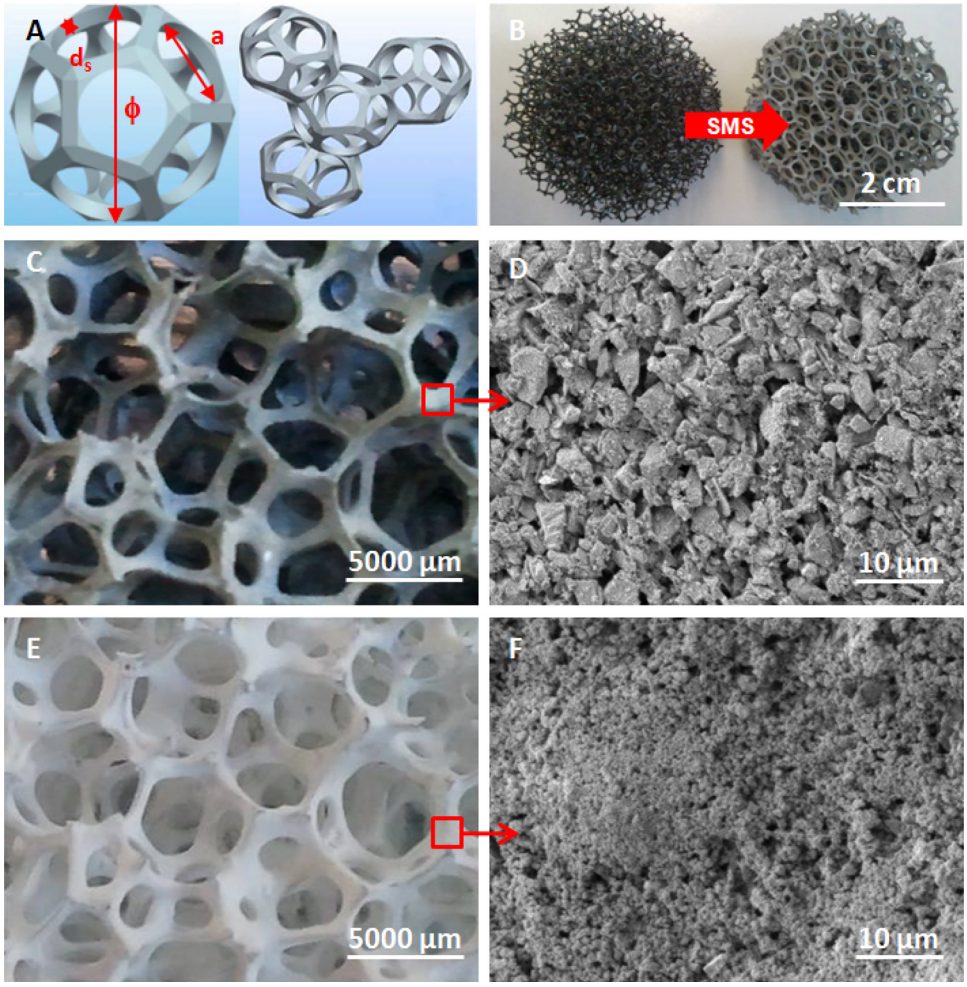


**Fig. 1.** (A) Schematic drawing of the model developed by Edouard, with packing of regular pentagonal dodecahedron [8,10], and characterized by the cell size (Φ), the strut or bridge diameter ($d_s$) and the window size or pore diameter (a) as their most characteristic parameters. (B) Optical images of the pre-shaped alveolar polyurethane precursor and the corresponding alveolar open-cell self-bonded β-SiC foam obtained through the shape memory synthesis (SMS) replica method. Optical and SEM images (C,D) of the bare medium specific surface area β-SiC foam and (E,F) of the $TiO_2$ UV100(15 wt.%)/β-SiC foam, in both cases with a 5400 µm mean cell size.

foams – mainly made of nickel or aluminum [13–17], and alumina or cordierite [18–24], respectively – and in a lesser extent to that of polymeric [11] and carbon foams [25,26]. However, they benefit from a high thermal and chemical stability, that allows the monolith to operate safely in severe basic or acidic reaction conditions. These properties also allow (if necessary) the easy regeneration of possibly deactivated supported photocatalysts to be performed without any irreversible damages, by thermal or soda-washing treatment. In addition, binder-free foams composed of self-bonded β-SiC grains can be easily manufactured with on-demand shapes for meeting the photoreactor geometry requirements through the implementation of the shape memory synthesis (SMS) replica method [27]. They also take advantage from a medium specific surface area for dispersing photocatalysts and from a high density of oxygenated surface groups for anchoring $TiO_2$ [28–30]. They differ, thus, from metallic foams, that usually suffer from their chemical nature and from a low specific surface area that needs to be increased by chemical and/or thermal pretreatments or by coating the foam with an oxide interlayer, in order to provide a better anchorage for the supported photocatalyst and to increase its density per foam unit volume. They differ also from oxide foams, that had relatively low surface area due to the high temperatures used for the ceramic shaping [2]. By contrast, secondary α-SiC foams commercialized as SiC filters suffer from very low surface area, the use of binders and limitations in terms of geometry availability.

Promising results have been obtained using β-SiC foams obtained by SMS as $TiO_2$ photocatalyst support, in liquid phase for continuous wastewater treatment taking the Diuron© pesticide as model compound [31,32] as well as in gas-phase for indoor air treatment [33], and results have been reported for the liquid phase ammonia degradation [34]. Recently, SiC foams composed of α-SiC, β-SiC and Si were used as $TiO_2$ support for degrading 4-aminobenzenesulfonic acid as model in water [35,36]. Powder SiC nanomaterials with different morphologies have also been used directly as UV or visible light photocatalysts [37–40] as well as within binary or ternary coupled systems with $TiO_2$ [41–43] or $TiO_2$–$WO_3$ [44].

This article reports on the use of alveolar open-cell self-bonded β-SiC foams with medium specific surface area and high open porosity as structured support for $TiO_2$ photocatalysts for gas phase applications, using as test reaction the degradation of gaseous butanone (Methylethylketone, MEK), a typical malodorous pollutant of dwelling house indoor air taken as gas phase model volatile organic compound [45]. Details on the mechanism of this well-documented reaction can be found in [45–47]. Commercially available $TiO_2$ Hombikat UV100, produced *via* the sulfate technology, was used as reference photocatalysts. The results are compared to those obtained with the commercial Quartzel® photocatalytic felt reference, designed for providing a very good light transmission inside the reactor core and for

allowing the reactor to operate in a flow-through mode at low pressure drop.

## 2. Experimental

### 2.1. Materials

Alveolar open-cell self-bonded β-SiC foams with medium specific surface area were synthesized by the SICAT Company (Willstätt, Germany) according to the shape memory synthesis (SMS) replica method, in which a pre-shaped polyurethane foam is transformed into the corresponding β-SiC carbide [27]. This method is a four step synthesis process, consisting in (i) the impregnation/infiltration of a pre-shaped precursor polyurethane foam with a phenolic resin containing micronized metallic silicon (<20 μm), (ii) a polymerization step at 150–250 °C, (iii) a reactive step at 1360 °C under argon, with the attack of carbon by SiO vapors formed by reaction between the silicon and the resin oxygenated compounds, to yield β-SiC, and (iv) a final thermal treatment in air at 700 °C for removing residual unreacted carbon by combustion. The method reflects the fact that the original macrostructural features of a solid, *i.e.* its macroscopic shape, were retained after synthesis. β-SiC foams can thus be manufactured with adjustable shapes suitable for being adapted to the photoreactor geometry and size. The starting polyurethane foam was used in the form of full disks and the resulting β-SiC disks were subsequently hollowed out so as to obtain ring-like shaped β-SiC foams (with 1.8 cm diameter inner hole) for filling the reactor and surrounding the lamp.

Commercial Hombikat UV100 $TiO_2$ photocatalyst was supplied by Sachtleben Chemie GmbH (Germany). Hombikat UV100 $TiO_2$ is composed of anatase as the sole crystallized phase, with a higher specific surface area of $330 \pm 15\ m^2\ g^{-1}$, micropores accounting for about $243\ m^2\ g^{-1}$, and features a smaller primary particle size of 8 nm. More details can be found in [32,48,49].

The deposition of the $TiO_2$ photocatalyst onto the alveolar β-SiC foam was performed by dipping the foam support into a $100\ g\ L^{-1}$ ethanolic $TiO_2$ suspension and further drying under airflow at 60 °C. The $TiO_2$ suspension was kept under stirring for 30 min before turning off the stirring for immerging the foam. The impregnation process was replicated, until the desired $TiO_2$ amount was obtained. The $TiO_2$/β-SiC foam was weighted after a final drying at 100 °C for determining the $TiO_2$ content, calculated relative to the total weight of the $TiO_2$/β-SiC foam.

The Quartzel® photocatalytic felt, supplied by Saint-Gobain-Quartz (France), is a 1 cm thick felt made from entangled 8–12 μm diameter Quartz fibers coated by sol–gel $TiO_2$. It had a total surface density of $120\ g\ m^{-2}$, including $40\ g\ m^{-2}$ of $TiO_2$, so that one single layer of Quartzel photocatalytic felt had a $TiO_2$ amount per unit volume of $4\ mg\ cm^{-3}$, also expressed as a $TiO_2$ surface density of $4\ mg\ cm^{-2}$.

### 2.2. Characterization techniques

Surface area measurements were carried out on a Micrometrics Tristar 3000 apparatus using $N_2$ as adsorbant at −196 °C, with a prior outgassing of the samples at 200 °C for 8 h for desorbing impurities or moisture. The BET specific surface area was calculated from the $N_2$ adsorption isotherms, the micropore surface area was derived using the *t*-plot method.

Scanning electron microscopy (SEM) was carried out in secondary electron mode on a JEOL-JSM-6700 F microscope equipped with a field emission gun and operating with an extraction potential ranging from 1 to 10 kV. Prior to analysis, the samples were coated with gold.

The light transmission through the β-SiC foams, the Quartzel® photocatalytic felt or the reactor coated $TiO_2$ films was defined as the fraction of the incident light, in terms of UV-A irradiance, being transmitted through the materials or the $TiO_2$ coating, by varying the foam thickness, the number of felt layers or the $TiO_2$ surface density of the reactor coating. UV-A irradiance measurements were performed using a wideband RPS900-W rapid portable spectroradiometer from International Light Technology.

### 2.3. Photocatalytic set-up, reactors and test procedures

#### 2.3.1. Single-pass tests

Two synthetic air flows were bubbled at ambient temperature and atmospheric pressure through two temperature-controlled saturators containing MEK (Sigma–Aldrich, 99%) and distilled water, respectively, and mixed with an additional synthetic air flow to set both MEK concentration and relative humidity (RH), as well as the total air flow rate. 100% of RH was defined as the saturated vapor pressure of water at 25 °C and atmospheric pressure, which corresponds to about 24 Torr, *i.e.* about 3% relatively to the total atmospheric pressure.

The photocatalytic performances were obtained by on-line quantifying both inlet and outlet flows with a R3000A micro-gas chromatograph (SRA-Instruments) with thermal conductivity microdetectors, allowing quantification of MEK, water, $CO_2$ and acetaldehyde. The single-pass efficiency of the remediation process was expressed in terms of MEK conversion ($C_{MEK}$), of selectivities to $CO_2$ ($S_{CO_2}$) and to acetaldehyde as main reaction intermediate byproduct ($S_{Ac}$), as well as of $CO_2$ mineralization yield, calculated according to Eqs. (1–4):

$$C_{MEK}(\%) = \frac{([MEK_{in}] - [MEK_{out}])}{[MEK_{in}]} \times 100 \quad (1)$$

$$S_{Ac}(\%) = \frac{[Ac_{out}]}{([MEK_{in}] - MEK_{out}) \times 2} \times 100 \quad (2)$$

$$S_{CO_2}(\%) = \frac{[CO_{2out}]}{([MEK_{in}] - [MEK_{out}]) \times 4} \times 100 \quad (3)$$

$$Y_{CO_2}(\%) = \frac{[CO_{2out}]}{[MEK_{in}] \times 4} \times 100 \quad (4)$$

The single-pass performances of the $TiO_2$/β-SiC foams were evaluated in tubular Pyrex reactors with a diameter of 4 cm and varying in terms of length, in which the photocatalytic foam rings were cast. The illumination was provided by a 26.5 cm length and 1.6 cm diameter UV-A lamp, located at the center of the tube and symmetrically surrounded by the $TiO_2$/β-SiC foam rings with a foam thickness around the lamp of 1.1 cm.

The influence of the $TiO_2$ weight content and of the mean cell size of the β-SiC foams was investigated in a 26.5 cm length reactor, corresponding to a total foam volume of $265\ cm^3$. The tests were performed at a MEK content of 1100 $ppm_v$, with 50% RH and a total air flow rate of $440\ mL\ min^{-1}$, corresponding to a residence time of 3 s and a velocity of $0.7\ cm\ s^{-1}$. The illumination was provided by a 8 W UV-A blacklight lamp (Sylvania Blacklight Blue F8W/BLB T5), with a spectral peak centered on 365 nm and an irradiance of $5.4\ mW\ cm^{-2}$ arriving at the external surface of foams.

Comparison was made with the reactor filled with layers of Quartzel® photocatalytic felt surrounding the axial lamp as well as with the foam-free reactor operating in a coated-wall mode, in which the $TiO_2$ photocatalyst was located as thin film on the inner side of the reactor tube [1,50].

The influence of reaction parameters (inlet MEK content and flow velocity) was studied in a 12.2 cm length reactor with an irradiance of $8.4\ mW\ cm^{-2}$ arriving at the external surface of foams, obtained with a 15 W UV-A blacklight lamp (Sylvania Blacklight F15W/T5/BLB350, spectral peak centered on 365 nm). The inlet MEK content was varying from 5 to 150 $ppm_v$, with a total air flow

of 20 L min$^{-1}$ corresponding to a residence time of 0.4 s and a flow velocity of 31.6 cm s$^{-1}$. The flow velocity was varying from 6.3 to 31.6 cm s$^{-1}$, with a total air flow rate ranging from 440 mL/min to 20 L/min, corresponding to residence times ranging from 3 s to 0.4 s, with an inlet MEK content of 75 ppm$_v$.

In single-pass test mode, photocatalytic materials and media were first exposed overnight to UV-A irradiation under air flow to remove ethanol solvent residues, and further exposed to the polluted air stream with no illumination until dark-adsorption equilibrium was reached, before the illumination was switched on.

### 2.3.2. Tests in a recirculation mode

Tests were performed in a 110 cm × 110 cm × 165 cm *(l × L × h)* parallelepipedic-shaped test chamber used as closed batch reactor, with an inner volume of 2 m$^3$, made of low adsorption chemically inert materials, and directly connected to the micro-gas chromatograph previously described for quantifying MEK and $CO_2$ as a function of time.

The photocatalytic reactor was similar than in the case of the single-pass mode tests, except the inlet of the reactor incorporated a fan (FD1260-C0151E/R2, ARX Ceradyna) operating at 4500 rpm and 33 m$^3$ h$^{-1}$. The reactor, thus, operated at a residence time of 0.014 s and a flow rate of 8.7 m s$^{-1}$. The illumination was provided by a 15 W UV-A blacklight lamp. After introduction of MEK inside the test chamber with a syringe and further homogenization of the chamber for 3 min performed using an additional fan operating at 33 m$^3$ h$^{-1}$, the photocatalytic reactor was turned on both in terms of lighting and of inlet fan. Comparison was also made with the same tubular reactor filled with layers of Quartzel® photocatalytic felt surrounding the axial lamp as well as with the reactor operating in the wall-coated reactor mode at the optimal $TiO_2$ surface density.

The tests were performed with 2–20 ppm$_v$ of MEK and 50% of relative humidity. At such initial MEK concentrations, the analytical system used was not sensitive enough for quantifying acetaldehyde reaction intermediate. The photocatalytic degradation kinetics of MEK were expressed by applying the Langmuir–Hinshelwood model for deriving the apparent rate constant, known to be a non-true apparent constant, taking into account that for highly diluted samples, the reaction is essentially an apparent first-order reaction [51].

## 3. Results and discussion

### 3.1. Characterization of the photocatalytic materials

The maintain of both the alveolar open-cell structure and the cell size of the foam during the SMS process going from polyurethane foam to β-SiC foam, is shown in Fig. 1B and Table 1. It evidenced the interest of using the flexible SMS replica method for manufacturing on-demand shape- and cell size-controlled β-SiC foam materials meeting the requirements of the photoreactor geometry by pre-shaping the precursor polyurethane foam with suitable cell properties.

β-SiC foams are labeled following their mean cell size, and had open porosity ranging from 0.91 ± 0.05 to 0.66 ± 0.05 for foams with mean cell size ranging from 5400 μm to 2900 μm. They had specific surface area ranging from 20 m$^2$ g$^{-1}$ to 35 m$^2$ g$^{-1}$. The geometrical specific surface area of the foams, derived from the open porosity and the mean strut diameter according to the model developed by Edouard and co-workers [10,12,52], was ranging from 620 ± 200 m$^{-1}$ for 5400 μm mean cell size to 4250 ± 700 m$^{-1}$ for 2900 μm mean cell size. The main characteristic parameters of the β-SiC foams are reported in Table 1. Taking β-SiC foams with 5400 μm mean cell size as example, supporting increasing amount of UV100 $TiO_2$ led to an increase of the surface area from 20 m$^2$/g for the bare foam to 69 m$^2$/g for the $TiO_2$(21 wt.%)/β-SiC foam photocatalyst, together with the mechanical increase in the microporous content issued from UV100 $TiO_2$ and the change of the isotherm curves (Supporting information S1).

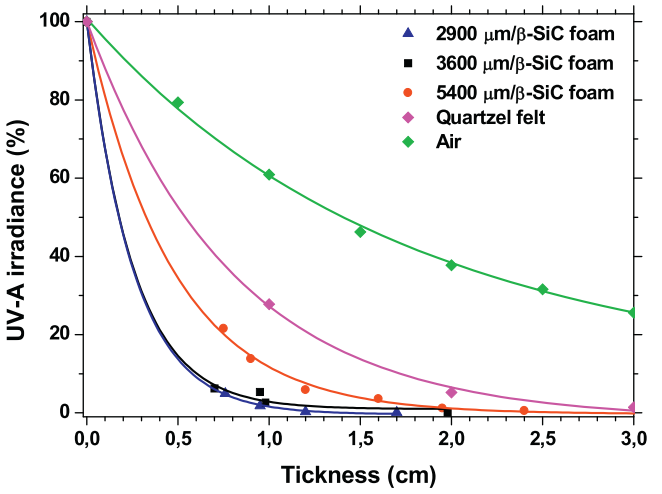


**Fig. 2.** UV-A light transmission within the β-SiC foam as a function of the foam thickness and of the mean cell size. The light transmission ability of β-SiC foams, expressed as the foam characteristic length (λ) was derived from a $T_t = e^{-t/\lambda}$ first order decreasing exponential model as a function of the foam thickness *t*. Comparison with the commercial Quartzel® photocatalytic felt and the natural decay of light irradiance in air.

XRD patterns of the β-SiC foam support and the $TiO_2$ UV 100/β-SiC foam photocatalysts shown in Supporting information S1 exhibited the diffraction lines attributed to the β-SiC polymorph in fcc structure (JCPDS Cards JCPDS 29-1129), as previously reported for β-SiC foams prepared *via* SMS [53,54], and in the case of $TiO_2$/foam materials, together with the diffraction peaks corresponding to anatase $TiO_2$ UV100 (JCPDS Card 21-1272, the most intense being the (1 0 1) diffraction peak at 25.3°).

Optical and SEM images of both β-SiC foam support and $TiO_2$ UV 100(15 wt.%)/β-SiC foam photocatalyst are shown in Fig. 2. They evidenced the homogeneity of the $TiO_2$ UV100 particle coating on the grainy and roughened surface of the β-SiC foam. The homogeneity of the coating was probably helped by the presence at the β-SiC surface, of a 1–4 nm thick amorphous layer composed of oxygenated phases such as $SiO_xC_y$ silicon oxycarbide and $SiO_2$ [28,29]. This layer improves the hydrophilic character of the support surface and acts as a natural washcoat layer for anchoring the catalyst to the surface [30,55–57].

The light transmission through the β-SiC foams as a function of the foam thickness is shown in Fig. 3 for foams with mean cell sizes ranging from 2900 μm to 5400 μm. They displayed a light transmission following a $T_t = e^{-t/\lambda}$ first order decreasing exponential model as a function of the foam thickness *t*, with λ representing the characteristic length for the corresponding β-SiC foam. Decreasing the mean cell size of the foam reduced the light transmission ability of the foam, with $\lambda_{2900} = 0{,}25 \pm 0{,}01$ cm, $\lambda_{3600} = 0{,}26 \pm 0{,}03$ cm and $\lambda_{5400} = 0{,}47 \pm 0{,}02$ cm (Table 1). However, this increases the geometrical specific surface area of the foam from 620 ± 200 m$^{-1}$ for 5400 μm mean cell size with 0.91 ± 0.05 open porosity to 4250 ± 700 m$^{-1}$ for 2900 μm mean cell size with 0.66 ± 0.05 open porosity, so that more $TiO_2$ particles could be activated by the UV-A light at the β-SiC foam surface. One should notice that, even for β-SiC foams with both larger cell size and open porosity, the light transmission ability remained lower than that shown by the commercial Quartzel® photocatalytic felt, known to be manufactured with a high light transmission ability in the UV-A range, with a $\lambda_{felt} = 0{,}8 \pm 0{,}06$ cm characteristic length.

**Table 1**
Some properties of alveolar β-SiC foams with mean cell sizes ranging from 2900 to 5400 μm, and their corresponding efficiency obtained in the single-pass MEK photocatalytic oxidation by supporting $TiO_2$ UV100 photocatalyst, as derived from Fig. 4.

| Foam label | β-SiC/2900 | β-SiC/3600 | β-SiC/5400 |
|---|---|---|---|
| | 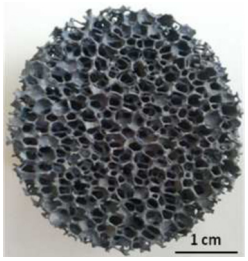  | 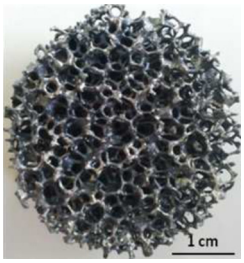  |   |
| Mean cell size ($\varphi$) (μm) | 2900 ± 220 | 3600 ± 400 | 5400 ± 700 |
| Equivalent PPI (pore per inch) | ≈15 | ≈13 | ≈8 |
| Window size ($a$) (μm) | 1400 ± 400 | 1600 ± 450 | 2300 ± 600 |
| Bridge diameter ($d_s$) (μm) | 320 ± 50 | 450 ± 70 | 575 ± 80 |
| Open porosity[a] | 0.66 ± 0.05 | 0.78 ± 0.05 | 0.91 ± 0.05 |
| λ (cm) | 0.25 ± 0.01 | 0.26 ± 0.03 | 0,47 ± 0,02 |
| Geometrical specific surface area ($m^{-1}$)[b] | 4250 ± 700 | 1955 ± 400 | 626 ± 200 |
| BET specific surface area ($m^2/g$) | 35 | 30 | 20 |
| Amount of $TiO_2$ UV100 on the plateau (mg), [$TiO_2$ content in wt.%] | 1500 [27] | 1000 [20] | 500 [13] |
| $TiO_2$ UV100 per reactor unit volume on the plateau ($mg/cm^3$) | 5.7 | 3.8 | 1.9 |
| MEK conversion and $CO_2$ mineralization yield on the plateau (%) | 40; 16 | 40; 16 | 35.9; 16 |

[a] measured by water displacement.
[b] derived from the model developed by Edouard and coll [10,12].

### 3.2. Alveolar $TiO_2$/β-SiC foam structured photocatalysts in single pass tests

The conversion, the selectivities to $CO_2$ and acetaldehyde, and the mineralization yield into $CO_2$ obtained at an inlet MEK concentration of 1100 $ppm_v$ and a flow rate of 440 mL $min^{-1}$ on the $TiO_2$ UV100/β-SiC foams (5400 μm mean cell size) as a function of the $TiO_2$ loading, are shown in Fig. 3. A first linear increase of MEK conversion and mineralization into $CO_2$ was observed with increasing the $TiO_2$ loading on the β-SiC foam before achieving a plateau. This behavior is similar to that observed in liquid and gas phase reactions with powder photocatalysts, due first to the increase in the amount of illuminated $TiO_2$ particles in the reactor, and further to a screening effect of excess particles, which mask part of the $TiO_2$ photocatalyst particles [58] – for gas phase applications – as a result from the limited penetration of UV-A light through the $TiO_2$ coating. A similar behavior was observed for the gas phase methanol degradation on carbon foam supported $TiO_2$ P25 photocatalyst [25] as well as for the Diuron® pesticide mineralization in water on β-SiC foam supported sol–gel $TiO_2$ [32].

On the plateau, a MEK conversion of 35.5% with a selectivity into $CO_2$ of 50% and mineralization rate of 18% was obtained on the UV100/β-SiC foam. With a level of 25% on the plateau, the evolution of the acetaldehyde selectivity with the increase of the $TiO_2$ amount followed the usual pattern corresponding to the evolution of an intermediate reaction by-product, with a decrease of the acetaldehyde selectivity for increased MEK conversions. A slight decrease in acetaldehyde selectivity was observed with the increase of the $TiO_2$ amount on the plateau, as a result from an artificial increase in the residence time of acetaldehyde within the photocatalytic coating. This could increase the probability of acetaldehyde to adsorb at the $TiO_2$ particle surface for reacting into another (non-detectable) intermediate by-product. This differs from the residence time within the reactor, set by the reaction conditions, and determined as the reactor volume-to-flow rate ratio.

First, it was necessary to proof the role of the β-SiC foam material by calculating the activity ratios between two $TiO_2$ photocatalysts (UV100 $TiO_2$ and Aeroxide $TiO_2$-P25 from Evonik) for both thin film reactors and β-SiC foam supported systems, for overcoming the fact that both configurations – β-SiC foam and thin film reactors – were operating in different reaction conditions (Supporting information S2). MEK conversions of 69% and 38% were achieved on the plateau for UV100 and P25 $TiO_2$ thin films, respectively, resulting in mineralization yields into $CO_2$ of 41.5% and 19.5%, respectively, while MEK conversions of 35.5% and 18.5% were achieved for β-SiC foam supported UV100 and P25 $TiO_2$ systems, respectively, resulting in mineralization yields into $CO_2$ of 18% and 8%, respectively (Supporting information S2). So, similar UV100/P25 activity ratios were obtained on thin films and on β-SiC foams, calculated for MEK conversion at 1.9 and 1.8, respectively, and for mineralization yield at 2.2 and 2.1, respectively. This indicated that the β-SiC foam material played here a passive role and that the superiority of the UV100/β-SiC foam photocatalyst resulted from the superiority of the UV100 coating toward the P25 coating, similarly to the case of powder thin films operating in the coated reactor wall mode. This differed from the recent results reported by Hao et al. who proposed a synergistic photocatalytic effect between the *p*-type semicondutive SiC foam and the *n*-type $TiO_2$ coating in $TiO_2$–SiC heterojunctions built by immobilization of $TiO_2$ nanoparticles on the SiC foam support [35].

Fig. 4 and Supporting information S3 show the influence of the mean cell size of the UV100/β-SiC foam on the performances of the UV100/β-SiC foams, expressed in terms of MEK conversion, selectivities to $CO_2$ and acetaldehyde, and mineralization yield into $CO_2$ obtained at an inlet MEK concentration of 1100 $ppm_v$ and a flow rate of 440 mL $min^{-1}$. They are reported directly as a function of the $TiO_2$ weight rather than of the $TiO_2$ weight percentage, due to the difference in terms of volume density between β-SiC foams with different mean cell sizes. At low $TiO_2$ weight content, increasing the mean cell size from 2900 μm to 5400 μm increased the MEK conversion, due to a strongly better light transmission, with *e.g.*, a MEK conversion of 24%, 28% and 31% being recorded at a $TiO_2$ weight of 250 mg with 2900 μm, 3600 μm and 5400 μm mean cell size foams. However, on the plateau level, the larger cell size foams displayed a slightly lower MEK conversion, at 36% for 5400 μm mean cell size, *vs.* 40% for 2900–3600 μm mean cell size. Larger cell size foams developed a smaller geometric surface, so that the plateau level in terms of performances was also achieved for a smaller $TiO_2$ weight content when increasing the mean cell size of the foams,

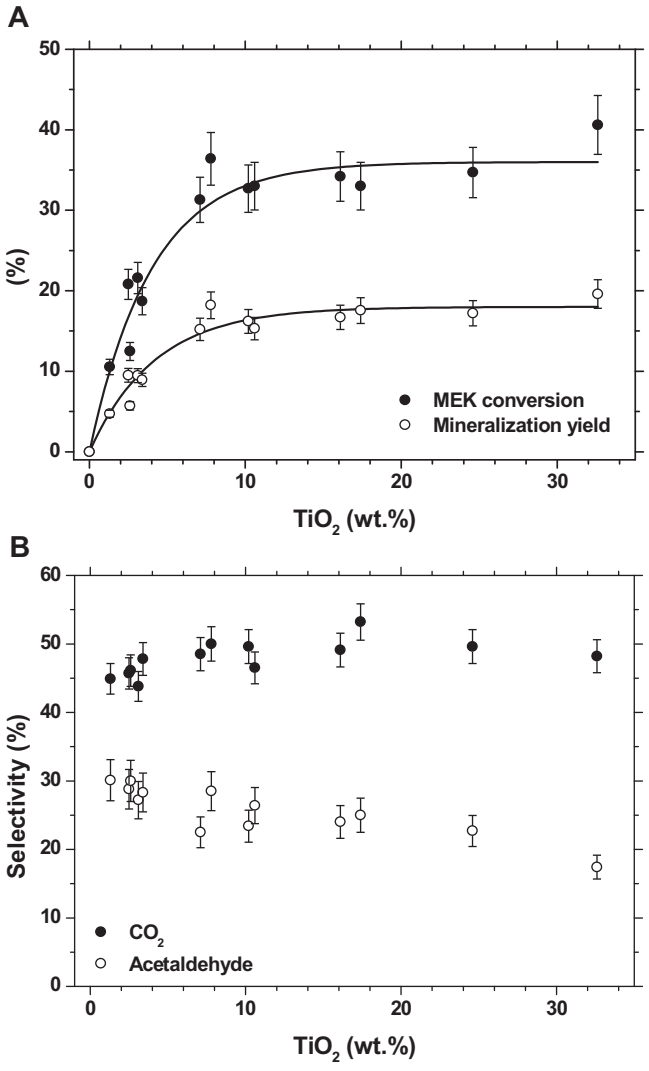


**Fig. 3.** Influence of the $TiO_2$ loading of the UV100/β-SiC foam photocatalysts (5400 μm mean cell size) on (A) the MEK conversion and the $CO_2$ mineralization yield, (B) both acetaldehyde and $CO_2$ selectivities. Reaction conditions: [MEK] = 1100 $ppm_v$, flow rate = 440 mL $min^{-1}$, velocity = 0.7 cm $s^{-1}$ and residence time = 3 s, 8 W UV-A light lamp, corresponding to an irradiance of 5.4 mW $cm^{-2}$ received by the external surface of the foams.

*i.e.* at approximatively 500 mg, 1000 mg and 1500 mg for mean cell sizes of 5400 μm, 3600 μm and 2900 μm, respectively, the screening effect being observed for lower $TiO_2$ weight contents on larger cell size foams. The higher MEK conversion for smaller mean cell size foams resulted probably from the compensation of the loss in light transmission when decreasing the mean cell size by the gain in available surface, so that larger amounts of $TiO_2$ could be immobilize per unit reactor volume on the plateau. This probably led to the increase in the amount of active $TiO_2$ – effectively irradiated by the light, even if with a weaker irradiance – within the coating.

In terms of selectivity, the decrease in the mean cell size from 5400 μm to 2900 μm resulted in a slight decrease in the $CO_2$ selectivity, from 50% to 46%, respectively. The slightly higher $CO_2$ selectivity on the larger cell size foams was attributed to the probably thicker $TiO_2$ coating on the plateau, that could result in an artificial increase in the residence time of intermediate by-products within the $TiO_2$ particle coating, improving the reaction toward full mineralization, like above-mentioned. As a result, the different the UV100/β-SiC foams discriminated in terms of mineralization yields – in favor of larger cell size β-SiC foam systems – before developing

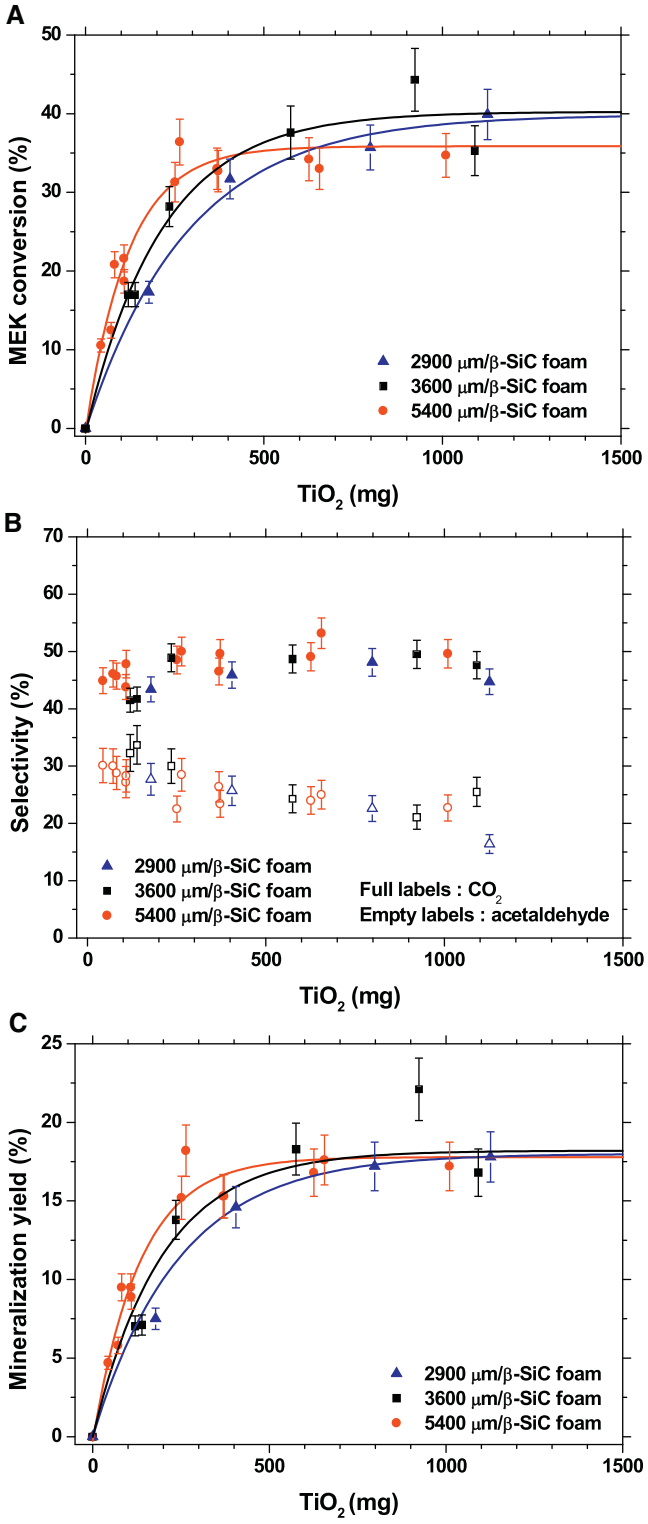


**Fig. 4.** Influence of the mean cell size of $TiO_2$ UV100/β-SiC foam in the 2900–5400 μm range, on (A) the MEK conversion, (B) both acetaldehyde and $CO_2$ selectivities and (C) the $CO_2$ mineralization yield, expressed as a function of the $TiO_2$ amount. Reaction conditions: [MEK] = 1100 $ppm_v$, flow rate = 440 mL $min^{-1}$, velocity = 0.7 cm $s^{-1}$ and residence time = 3 s; 8 W UV-A light lamp, corresponding to an irradiance of 5.4 mW $cm^{-2}$ received by the external surface of the foams.

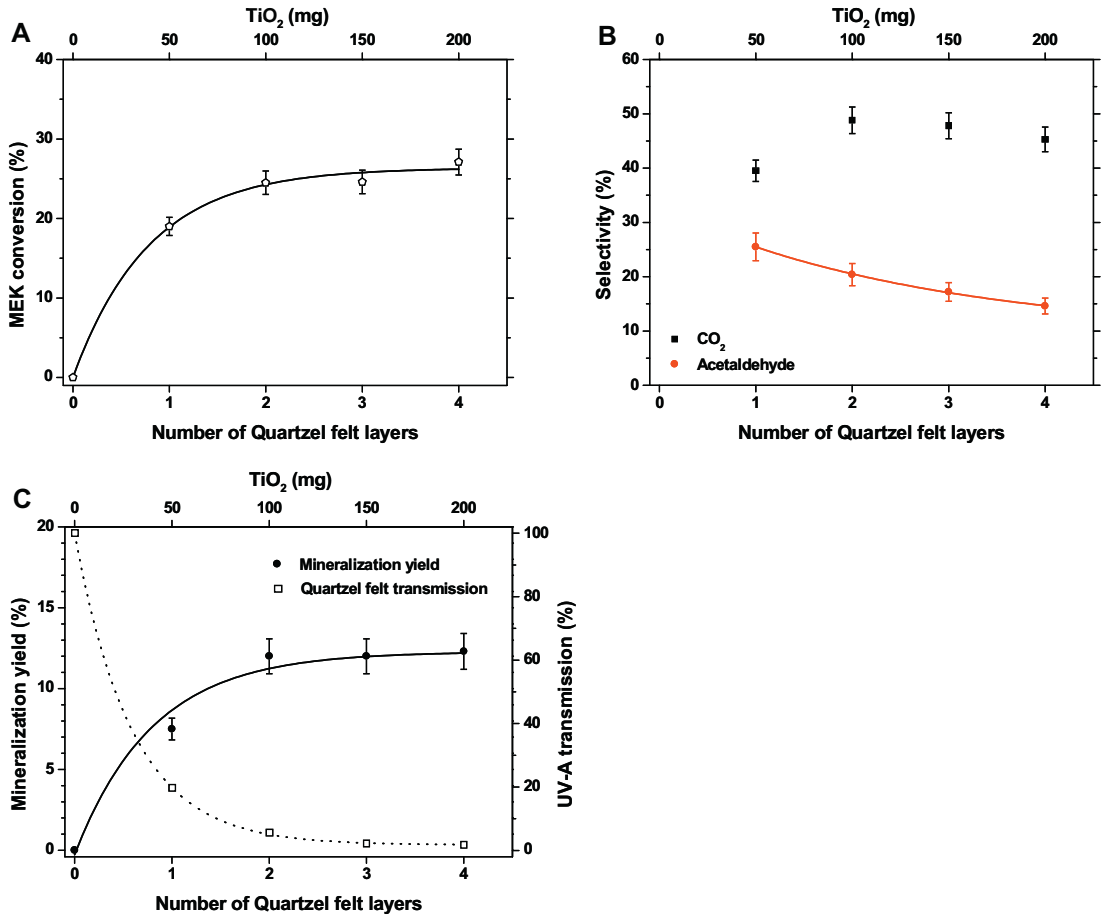


**Fig. 5.** Influence of the number of Quartzel® photocatalytic felt layers surrounding the UV-A lamp in the reactor on (A) the MEK conversion, (B) both acetaldehyde and $CO_2$ selectivities (%) and (C) the $CO_2$ mineralization yield (%) and the UV-A light transmission through the felt layers. Reaction conditions: [MEK] = 1100 $ppm_v$, flow rate = 440 mL $min^{-1}$, velocity = 0.7 cm $s^{-1}$ and residence time = 3 s; 8 W UV-A lamp, corresponding to an irradiance of 5.4 mW $cm^{-2}$ received by the external surface of the rolled felt. Each felt layer has a length of 2.2 cm with a geometric surface of 12 ± 1 $cm^2$ so that it contained 50 ± 4 mg of $TiO_2$.

on the plateau level a similar mineralization yield of 16% whatever the mean cell size.

Fig. 5 shows the influence of the number of Quartzel photocatalytic felt layers surrounding the lamp within the reactor, on the MEK conversion, the $CO_2$ and acetaldehyde selectivities and the mineralization yield into $CO_2$ obtained in a single pass mode at an inlet MEK concentration of 1100 $ppm_v$ and a flow rate of 440 mL/min. The increase in the number of layers – and as a result in the amount of $TiO_2$ also reported in Fig. 5 – led to the increase of the overall performances, with a first increase of both MEK conversion and $CO_2$ mineralization yield due to the increase in the amount of illuminated $TiO_2$ particles, before they stabilized for more than two layers of felt at levels of 26.2% and 12.2%, respectively, as a result of the screening effect of excess particles and fibers, which masks part of the $TiO_2$ particles due to the limited penetration thickness of UV-A illumination. Indeed, measurements of light transmission through the photocatalytic felt layers evidenced that the light transmission efficiency dropped down very rapidly even through one single felt layer, and that only 5.6% of the incident light was transmitted through two layers of felt rolled within the reactor, corresponding to 100 mg of $TiO_2$ (Fig. 5C). Taking that into account, further comparisons in single-pass mode as well as in recirculation mode were performed with one and two layers of Quartzel photocatalytic felt rolled around the lamp for filling the reactor volume, two layers being considered as optimal operating conditions in this configuration.

The influence of the MEK concentration and of the residence time on the reactor efficiency for the different systems operating in optimal conditions is shown in Fig. 6, namely the UV100(16 wt.%)/β-SiC foam with 5400 μm mean cell size containing 3000 mg of $TiO_2$ UV100, UV100 powder thin film at 2 mg $cm^{-2}$ operating in a coated wall mode and exposing 300 mg of $TiO_2$, and 2 layers of Quartzel photocatalytic felt containing 680 mg of $TiO_2$ (170 $cm^2$ of felt). For comparison, the results obtained with one single layer of Quartzel photocatalytic felt containing 340 mg of $TiO_2$ (85 $cm^2$ of felt) are also reported.

Fig. 6A shows the influence of the MEK concentration within the 5–150 $ppm_v$ range at a residence time of 0.4 s (total air flow of 20 L $min^{-1}$) on the MEK conversion, and evidenced the interest of using the UV100/β-SiC foam structured photocatalyst compared to the coated-wall reactor and to the Quartzel photocatalytic felt. It was worth nothing that, lower the inlet MEK concentration, more pronounced the superiority of the β-SiC foam supported photocatalyst, so that the UV100/β-SiC foam structured photocatalyst is especially promising for indoor air treatment applications, for which very low concentrations of pollutant are concerned, *i.e.*, lower than 1 $ppm_v$.

Fig. 6B shows the influence of the residence time within the 2–0.4 s range (corresponding to the 4–20 L $min^{-1}$ range in terms of air flow rate) at a inlet MEK concentration of 75 $ppm_v$, on the MEK conversion, expressed in terms of μmol $min^{-1}$ of MEK converted. The different systems exhibited a similar behavior with

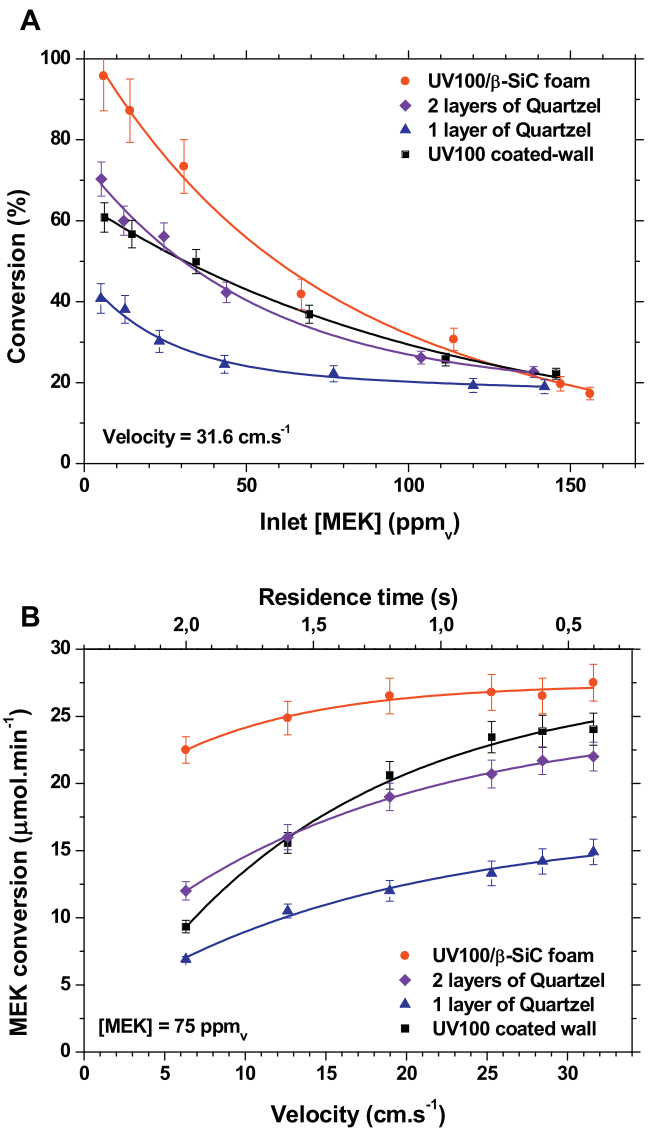


**Fig. 6.** Influence of (A) the MEK concentration and (B) the air velocity on the reactor efficiency for the $TiO_2$ UV100(16 wt.%)/β-SiC foam structured photocatalyst with a 5400 μm mean cell size, 1 and 2 layers of Quartzel photocatalytic felt and the $TiO_2$ UV100 coated-wall reactor operating at 2 mg cm$^{-2}$, expressed in terms of MEK conversion and of amount of degraded MEK, respectively. Reaction conditions: [MEK] = 5–150 ppm$_v$, flow rate = 4–20 L min$^{-1}$, velocity = 6,3–31,6 cm s$^{-1}$ and residence time = 2–0.4 s; 15 W UV-A lamp with an irradiance of 8.4 mW cm$^{-2}$.

decreasing the residence time, with an increase in the amount of MEK converted per minute to achieve a plateau level. They discriminate at the larger residence time, as well as on the plateau, and the efficiency difference is progressively reduced with reducing the residence time, the β-SiC foam structured photocatalyst, the coated wall reactor, and one and two Quartzel photocatalytic felts enabling the conversion, respectively, of 22.5, 9.3, 6.9 and 12.0 μmol min$^{-1}$ of MEK at a residence time of 2 s, before stabilizing their efficiency at 27.5, 24.0, 14.9 and 22.0 μmol min$^{-1}$ of MEK on the plateau at a residence time of 0.4 s. This evidenced first the superiority of the β-SiC foam supported photocatalyst compared to the other configurations. Secondly, it was noteworthy that the β-SiC foam supported photocatalyst enabled to turn from the diffusionnal – for which the performances are limited by mass transfer from gas phase to the photocatalyst surface – to the kinetic regime, at a lower flow rate (*i.e.*, for a higher residence time) than the coated wall reactor and the Quartzel photocatalytic felt systems.

The catalytic behavior of the β-SiC foam supported photocatalyst at low pollutant concentrations and at a lower flow rate compared to the other configurations was attributed to the static mixer effect played by the foam support. The small thickness of the struts constituting the solid foams are beneficial to mass transfer properties [10,12,52], and solid foam structures have been reported to allow a significant improvement in the mixing, especially in direction perpendicular to the flow due to the continuous impact between the flow and the support struts which generates turbulences within the flow pattern [59]. So, the $TiO_2$/β-SiC foam system takes advantage from this property intrinsic to open-cell solid foams at low flow rate and at low pollutant concentration.

### 3.3. Alveolar $TiO_2$/β-SiC foam structured photocatalysts in recirculation tests

Fig. 7 shows the evolution of the MEK concentration for an initial concentration within the 2–20 ppm$_v$ range for the different systems operating in optimal conditions: the UV100(16 wt.%)/β-SiC foam with 5400 μm mean cell size containing 3000 mg of $TiO_2$ UV100, UV100 powder coating at 2 mg cm$^{-2}$ operating in a coated wall mode and exposing 300 mg of $TiO_2$, and 2 layers of Quartzel photocatalytic felt containing 680 mg of $TiO_2$ (170 cm$^2$ of felt). For comparison, the results obtained with one single layer of Quartzel photocatalytic felt containing 340 mg of $TiO_2$ (85 cm$^2$ of felt) are also reported. Previous results showed that homogenization occurred in the chamber volume within less than 1 min, in agreement with simulation results on the velocity field distribution inside the chamber, based on fluid mechanics Navier–Stokes equations [33].

First, blank tests performed in the absence of photocatalyst showed the stability of the MEK concentration at 20 ± 0.5 ppm$_v$, 5 ± 0.1 ppm$_v$ and 2 ± 0.07 ppm$_v$ during the course of the tests, so that it was not necessary to introduce any chamber leakage effect within the first-order apparent rate constant, similarly to results obtained by Kartheuser et al. [60].

The Langmuir–Hinshelwood model linear regression derived from experimental degradation data is shown in Supporting information S4 and the apparent kinetic rate constants are reported in Table 2. Whatever the initial MEK concentration, the apparent kinetic rate constants highlighted the superiority of the UV100(16 wt.%)/β-SiC foam photocatalyst with 5400 μm mean cell size and the different systems were ranked as follows: UV100/β-SiC foam > 2 layers of photocatalytic felt > 1 layer of photocatalytic felt > UV100 coated wall reactor. For instance, at an initial MEK concentration of 5 ppm$_v$, UV100/β-SiC foam yielded a complete degradation of MEK within 5.5 h under recirculation, whereas 10 h was necessary using 2 layers of photocatalytic felt, and only 95% and 91.6% of MEK conversion was achieved after 11 h under recirulation using a single layer of photocatalytic felt and the UV100 coated wall reactor, respectively. At the highest initial MEK concentration of 20 ppm$_v$, UV100/β-SiC foam yielded a complete degradation of MEK within 10 h under recirculation, whereas 15 h and 19 h were necessary using 2 and 1 layers of photocatalytic felt, respectively, and 22.5 h was necessary using the UV100 coated wall reactor.

The evolution of both $CO_2$ concentration and $CO_2$ mineralization yield as a function of time under recirculation is also reported in the case of the test at high initial MEK concentration, due to sensitivity limitation for lower concentration levels. Chum et al. reported formation of acetaldehyde, acetone, methanol, ethane, methane and acetic acid [61]. Raillard et al. detected acetaldehyde, acetone and methanol [47,62,63]. More recently, Vincent et al. only detected acetaldehyde as by-product of MEK photocatalytic degradation [45,64]. One should note that no acetaldehyde (primary MEK reaction intermediate) was detected the in gas phase in our test conditions with our analytical systems. Taking the

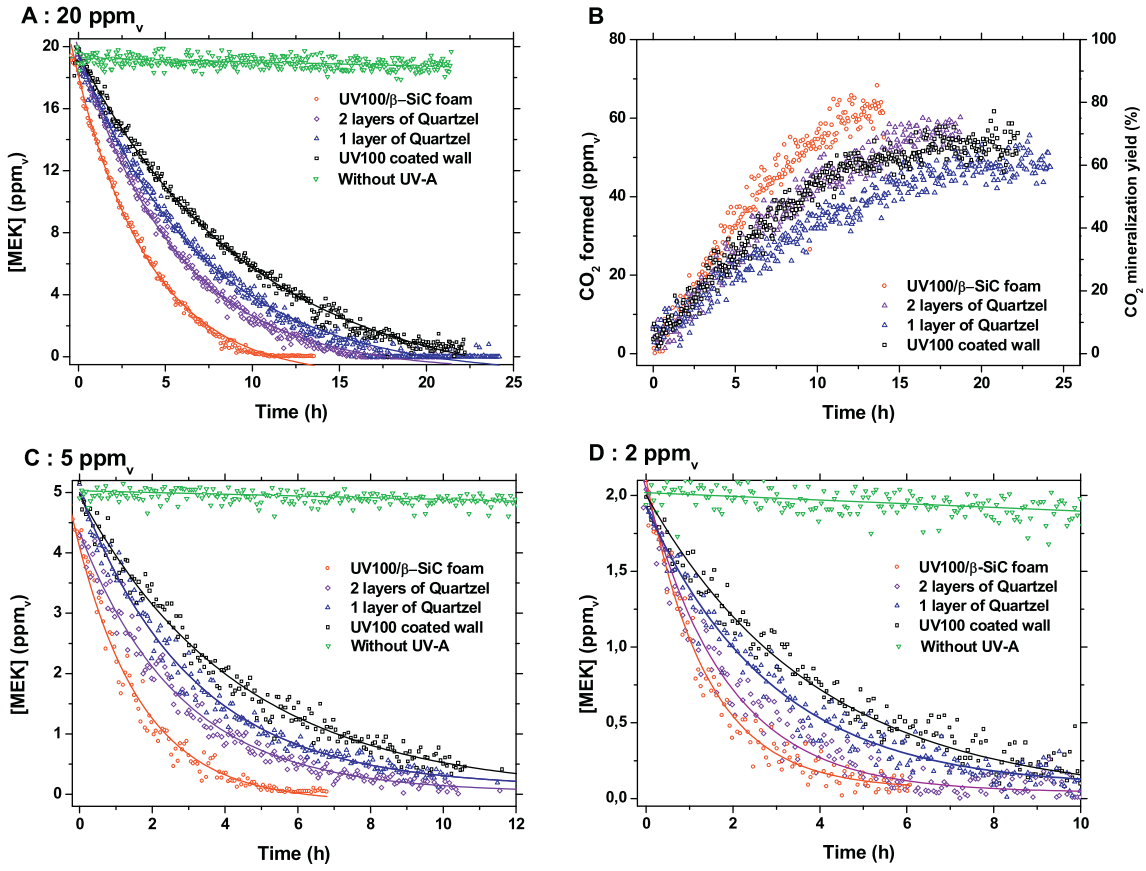


**Fig. 7.** Relative evolution of the MEK concentration with time under recirculation, for the $TiO_2$ UV100(16 wt.%)/β-SiC foam structured photocatalyst with a 5400 μm mean cell size, 1 and 2 layers of Quartzel photocatalytic felt and the $TiO_2$ UV100 coated-wall reactor operating at 2 mg cm$^{-2}$, with an initial MEK concentration of (A) 20 ppm$_v$, (C) 5 ppm$_v$ and (D) 2 ppm$_v$. (B) The evolution of the $CO_2$ concentration with time under recirculation over the different systems is also reported for an initial MEK concentration of 20 ppm$_v$.
Reaction conditions: [MEK] = 2–20 ppm$_v$, flow rate = 33 m$^3$ h$^{-1}$, velocity = 8,7 m s$^{-1}$ and residence time = 0,014 s; 15 W UV-A lamp with an irradiance of 8.4 mW cm$^{-2}$.

example of the β-SiC foam-based photocatalyst, it was noteworthy that the $CO_2$ concentration still increased after complete MEK oxidation occurred, *i.e.*, for duration longer than 10 h, as a result from the further oxidation of partially oxidized reaction intermediates. So, the mineralization yield to $CO_2$ was close to 80% after 15 h of operation. The remaining 20% to close the carbon balance were probably other reaction intermediates that required longer operation durations for being fully mineralized. However, it has to be mentioned that lower mineralization yields were obtained with the Quartzel photocatalytic felt layers in comparison to the UV100 coated wall reactor, even when full MEK conversion was achieved. This could be attributed to the nature of the $TiO_2$ photocatalyst covering the Quartz fibers, *i.e.*, sol–gel $TiO_2$ *vs.* $TiO_2$ UV100, that probably displayed different surface properties, in terms of reaction intermediate adsorption especially, resulting in a less selective process.

The apparent kinetic rate constants derived from tests with the highest MEK initial concentration, *i.e.*, 20 ppm$_v$, were clearly lower than those derived from tests at 2 and 5 ppm$_v$, whatever the reactor configuration. This could be explained by the formation of much larger amounts of reaction intermediates with a better affinity with the $TiO_2$ surface than MEK, and that would lead to deviate from the validity of the LH model assumptions. The presence of such intermediates in higher contents could then modify the coverage rates of the surface with MEK reactant and reaction intermediates. This effect was more pronounced for the β-SiC foam-based photocatalyst that displayed the highest activity. Models taking into account adsorption competition between MEK reactant and reaction intermediates for the same $TiO_2$ site could be introduced for explaining the deviation from the L–H model [45]. In this approach, Vincent et al. evidenced that MEK and acetaldehyde were not in competition on the same $TiO_2$ surface site [45], but other non-detectable reaction intermediates resulting from the oxidation of MEK could.

The comparison of the different systems at a similar $TiO_2$ loading in weight, *i.e.*, for the same amount of $TiO_2$ per unit reactor

**Table 2**
Apparent kinetic rate constant derived from the Langmuir–Hinshelwood model for the UV100/β-SiC foam structured photocatalyst (5400 μm, $TiO_2$ 16 wt.%), 1 and 2 layers of Quartzel® photocatalytic felt and the UV100 coated wall reactor at 2 mg cm$^{-2}$. Reaction conditions: [MEK] = 2–20 ppm$_v$, flow rate = 33 m$^3$/h, velocity = 8,7 m s$^{-1}$ and residence time = 0,014 s; 15 W UV-A lamp with an irradiance of 8.4 mW cm$^{-2}$.

| | Initial MEK concentration (ppm$_v$) | UV100/β-SiC (5400 μm, 16 wt.% $TiO_2$) | Quartzel® felt (1 layer) | Quartzel® felt (2 layers) | UV100 coated wall reactor (2 mg cm$^{-2}$) |
|---|---|---|---|---|---|
| Apparent kinetic rate constant (h$^{-1}$) | 2 | 0.72 | 0.32 | 0.48 | 0.25 |
| | 5 | 0.72 | 0.30 | 0.37 | 0.23 |
| | 20 | 0.26 | 0.15 | 0.18 | 0.12 |

volume, pointed out logically that the $TiO_2$ coated wall reactor configuration is the most efficient, due to a better illumination of $TiO_2$ particles when compared to the β-SiC foam structured reactor. By contrast, implementing the different systems at their optimal operating conditions highlighted that the structured β-SiC foam photocatalytic materials take advantage of the static mixer effect and of their ability to increase the amount of $TiO_2$ per unit reactor volume for overcoming the weaker irradiance received by the $TiO_2$ particle coating in the core of the reactor.

## 4. Conclusion

Alveolar open-cell self-bonded β-SiC foams with medium specific surface area have been successfully used as structured support for $TiO_2$ photocatalyst in the gas phase photocatalytic degradation of methylethylketone. The interest of using high open porosity $TiO_2$/β-SiC foams with large 5400 μm mean size cells operating in a flow-through reactor was highlighted in a single-pass mode as well as in recirculation mode within a test chamber. The structured β-SiC foam photocatalytic materials take advantage of a static mixer effect and of their ability to increase the amount of $TiO_2$ per unit reactor volume for overcoming the weaker irradiance received by the $TiO_2$ particle coating in the core of the reactor.

Implementing the different photocatalytic systems at their optimal operating conditions evidenced the superiority of the structured photocatalytic materials against the commercially available Quartzel photocatalytic felt standard and the thin film coated wall reactor. It was all the more pronounced than the pollutant concentration and the air flow rate were decreased, so that photocatalytic reactors structured with $TiO_2$/β-SiC foams could thus be promising for indoor air remediation, especially, by taking advantage of the static mixer role played by the β-SiC foam support.

No synergistic photocatalytic effect was observed between *p*-type semiconductive SiC foam and *n*-type $TiO_2$ photocatalyst, so that the β-SiC foam material played here a passive role of photocatalyst support and static mixer.

## Acknowledgements

French ANRT and CIFRE program are thanked for financial support. Thierry Romero is acknowledged for performing the SEM analysis. Alain Rach is thanked for helping in implementing the different photocatalytic reactors and the photocatalytic set-up. SICAT Catalyst is thanked for providing the β-SiC foams.

## Appendix A. Supplementary data

Supplementary data associated with this article can be found, in the online version, at http://dx.doi.org/10.1016/j.apcatb.2015.01.030.

## References

[1] H. De Lasa, B. Serrano, M. Salaices, Photocatalytic Reaction Engineering, Springer, New York, 2005, pp. 17–47.
[2] D. Robert, V. Keller, N. Keller, in: P. Pichat (Ed.), Photocatalysis and Water Purification, From Fundamentals to Recent Applications, Wiley-VCH, Weinheim, 2013, pp. 145–178.
[3] T. Ochiai, A. Fujushima, J. Photochem. Photobiol. C: Photochem. Rev. 13 (2012) 247.
[4] K. Nakata, A. Fujushima, J. Photochem. Photobiol. C: Photochem. Rev. 13 (2012) 169.
[5] M.M. Hossain, G.B. Raupp, S.O. Hay, T.N. Obee, AIChE J. 45 (1999) 1309–1321.
[6] J. Taranto, D. Frochot, P. Pichat, Catal. Today 122 (2007) 66–77.
[7] T.N. Obee, R.T. Brown, Environ. Sci. Technol. 29 (1995) 1223–1231.
[8] G. Groppi, E. Tronconi, Chem. Eng. Sci. 55 (2000) 2161–2171.
[9] J.T. Richardson, Y. Peng, D. Remue, Appl. Catal. A: Gen. 204 (2000) 19–32.
[10] D. Edouard, M. Lacroix, C. Pham, M. Mbodji, C. Pham-Huu, AIChE J. 54 (2008) 2823–2832.
[11] S. Josset, S. Hajiesmaili, D. Begin, D. Edouard, C. Pham-Huu, M.-C. Lett, N. Keller, V. Keller, J. Hazard. Mater. 175 (2010) 372–381.
[12] T.T. Huu, M. Lacroix, C. Pham Huu, D. Schweich, D. Edouard, Chem. Eng. Sci. 64 (2009) 5131–5142.
[13] Z. Xiong, G. Zhang, L. Xiong, L. Fu, H. Pan, Appl. Mech. Mater. 71–78 (2011) 2944–2947.
[14] S. Zhu, X. Yang, W. Yang, L. Zhang, J. Wang, M. Huo, Int. J. Environ. Res. Public Health 9 (2012) 548–563.
[15] J. Yuan, H. Hu, M. Chen, J. Shi, W. Shangguan, Catal. Today 139 (2008) 140–145.
[16] G. Plantard, V. Goetz, F. Correia, J.P. Cambon, Sol. Energy Mater. Sol. Cells 95 (2011) 2437–2442.
[17] X. Wang, F. Han, X. Wang, Y. Li, Mater. Chem. Phys. 145 (2014) 68–74.
[18] G.B. Raupp, A. Alexiadis, M.M. Hossain, R. Changrani, Catal. Today 69 (2001) 41–49.
[19] S. Qiu, S. Xu, F. Ma, J. Yang, Powder Technol. 210 (2011) 83–86.
[20] M. Vargova, G. Plesch, U.F. Vogt, M. Zahoran, M. Gorbar, K. Jesenak, Appl. Surf. Sci. 257 (2011) 4678–4684.
[21] Y. Yao, T. Ochiai, H. Ishiguro, R. Nakano, Y. Kubota, Appl. Catal. B: Environ. 106 (2011) 592–599.
[22] S. Kato, Y. Hirano, M. Iwata, T. Sano, K. Takeuchi, S. Matsuzawa, Appl. Catal. B: Environ. 57 (2005) 109–115.
[23] I.J. Ochuma, O.O. Osibo, R.P. Fishwick, S. Pollington, A. Wagland, J. Wood, J.M. Winterbottom, Catal. Today 128 (2007) 100–107.
[24] H. Ishiguro, Y. Yao, R. Nakano, M. Hara, K. Sunada, K. Hashimoto, J. Kajioka, A. Fujishima, Y. Kubota, Appl. Catal. B: Environ. 129 (2013) 56–61.
[25] S. Hajiesmaili, S. Josset, D. Bégin, C. Pham-Huu, N. Keller, V. Keller, Appl. Catal. A: Gen. 382 (2010) 122–130.
[26] L.F. Velasco, B. Tsyntsarski, B. Petrova, T. Budinova, N. Petrov, J.B. Parra, C.O. Ania, J. Hazard. Mater. 184 (2010) 843–848.
[27] P. Nguyen, C. Pham, Appl. Catal. A: Gen. 391 (2011) 443–454.
[28] N. Keller, F. Di Grégorio, C. Pham-Huu, V. Keller, Diamond Relat. Mater. 17 (2008) 1867–1870.
[29] N. Keller, C. Pham-Huu, S. Roy, M.J. Ledoux, C. Estournes, J. Guille, J. Mater. Sci. 34 (1999)
3189–3202.
[30] N. Keller, C. Pham-Huu, C. Estournès, M.J. Ledoux, Appl. Catal. A: Gen. 234 (2002) 191–205.
[31] N.A. Kouamé, D. Robert, V. Keller, N. Keller, C. Pham, P. Nguyen, Catal. Today 161 (2011) 3–7.
[32] N.A. Kouamé, D. Robert, V. Keller, N. Keller, C. Pham, P. Nguyen, Environ. Sci. Pollut. Res. 19 (2012) 3727–3734.
[33] N. Doss, P. Bernhardt, T. Romero, R. Masson, V. Keller, N. Keller, Appl. Catal. B: Environ. 154–155 (2014) 301–308.
[34] P. Rodriguez, V. Meille, S. Pallier, M. Ali Al Sawah, Appl. Catal. A: Gen. 360 (2009) 154–162.
[35] D. Hao, Z. Yang, C. Jiang, J. Zhang, Appl. Catal. B: Environ. 144 (2013) 196–202.
[36] D. Hao, Z. Yang, C. Jiang, J. Zhang, J. Mater. Sci. Technol. 29 (2013) 1074–1078.
[37] O. Haibo, H. Jianfeng, Z. Xierong, C. Liyun, L. Cuiyan, X. Xinbo, F. Jie, Ceram. Int. 40 (2014) 2619–2625.
[38] J. Zhang, J. Chen, L. Xin, M. Wang, Mater. Sci. Eng.: B 179 (2014) 6–11.
[39] J.-Y. Hao, Y.-Y. Wang, X.-L. Tong, G.-Q. Jin, X.-Y. Guo, Catal. Today 212 (2013) 220–224.
[40] W. Zhou, L. Yan, Y. Wang, Y. Zhang, Appl. Phys. Lett. 89 (2006).
[41] T. Zou, C. Xie, Y. Liu, S. Zhang, Z. Zou, S. Zhang, J. Alloys Compd. 552 (2013) 504–510.
[42] H. Yamashita, Y. Nishida, S. Yuan, K. Mori, M. Narisawa, Y. Matsumura, T. Ohmichi, I. Katayama, Catal. Today 120 (2007) 163–167.
[43] Y. Nishida, T. Omichi, I. Katayama, H. Yamashita, M. Narisawa, Y. Matsumura, e-J. Surf. Sci. Nanotechnol. 3 (2005).
[44] V. Keller, F. Garin, Catal. Commun. 4 (2003) 377–383.
[45] G. Vincent, A. Queffeulou, P.M. Marquaire, O. Zahraa, J. Photochem. Photobiol. A: Chem. 191 (2007) 42–50.
[46] G. Vincent, P.M. Marquaire, O. Zahraa, J. Photochem. Photobiol. A: Chem. 197 (2008) 177–189.
[47] C. Raillard, V. Hequet, P.L. Cloirec, J. Legrand, Appl. Catal. B: Environ. 59 (2005) 213–220.
[48] G. Colón, M.C. Hidalgo, J.A. Navío, J. Photochem. Photobiol. A: Chem. 138 (2001) 79–85.
[49] J. Kirchnerova, M.L. Herrera Cohen, C. Guy, D. Klvana, Appl. Catal. A: Gen. 282 (2005) 321–332.
[50] Y. Paz, Adv. Chem. Eng. 36 (2009) 289–336.
[51] J.-M. Herrmann, Appl. Catal. B: Environ. 99 (2010) 461–468.
[52] M. Lacroix, P. Nguyen, D. Schweich, C. Pham Huu, S. Savin-Poncet, D. Edouard, Chem. Eng. Sci. 62 (2007) 3259–3267.
[53] M.J. Ledoux, C. Pham-Huu, CaTTech 5 (4) (2001) 226.
[54] E. Vanhaecke, S. Ivanova, A. Deneuve, O. Ersen, D. Edouard, G. Winé, P. Nguyen, C. Pham, C. Pham-Huu, J. Mater. Chem. 18 (2008) 4654.
[55] G. Rebmann, V. Keller, M.J. Ledoux, N. Keller, Green Chem. 10 (2008) 207–213.
[56] G. Winé, J.-P. Tessonnier, S. Rigolet, C. Marichal, M.-J. Ledoux, C. Pham-Huu, J. Mol. Catal. A: Chem. 248 (2006) 113–120.
[57] S. Ivanova, B. Louis, B. Madani, J.P. Tessonnier, M.J. Ledoux, C. Pham-Huu, J. Phys. Chem. C 111 (2007) 4368–4374.
[58] J.-M. Herrmann, Catal. Today 53 (1999) 115–129.
[59] Y. Liu, S. Podila, D.L. Nguyen, D. Edouard, P. Nguyen, C. Pham, M.J. Ledoux, C. Pham-Huu, Appl. Catal. A: Gen. 409–410 (2011) 113–121.

[60] B. Kartheuser, N. Costarramone, T. Pigot, S. Lacombe, Environ. Sci. Pollut. Res. 19 (2012) 3763–3771.
[61] H.L. Chum, M. Ratcliff, F.L. Posey, J.A. Turner, A.J. Nozik, J. Phys. Chem. 87 (1983) 3089–3093.
[62] C. Le Bideau-Raillard. Oxydation photocatalytique de composés organiques volatils. Thèse de l'Université de Nantes (2004).
[63] C. Le Bideau-Raillard, V. Hequet, P. Le Cloirec, J. Legrand, Water Sci. Technol. 50 (2004) 241–250.
[64] G. Vincent. Procédés d'élimination de la pollution de l'air par traitement photocatalytique: application aux COVs, Thèse de l'Université de Nancy (2008).